Supporting information

TITLE

Rigorous analysis of the interaction between proteins and low water-solubility drugs by qNMR-aided NMR titration experiments

AUTHORS

Takuya Hirakawa, Erik Walinda, Daichi Morimoto, Kenji Sugase[*]

AFFILIATIONS

[*] T. Hirakawa, Dr. D. Morimoto, Prof. K. Sugase

Department of Molecular Engineering, Graduate School of Engineering, Kyoto University, Kyoto University, Kyoto-Daigaku Katsura, Nishikyo-Ku, Kyoto 615-8510 (Japan)

E-mail: sugase@moleng.kyoto-u.ac.jp

Dr. E. Walinda

Department of Molecular and Cellular Physiology, Graduate School of Medicine, Kyoto University, Yoshida Konoe-cho, Sakyo-ku, Kyoto 606-8501 (Japan)

Table of Contents

1 General

1.1 Materials

[*U*-^{15}N]- and [*U*-^{13}C; *U*-^{15}N]-FKBP12 were prepared as reported previously[1]. Pimecrolimus (Figure S1) and BSA were purchased from Sigma Aldrich and Nacalai tesque, respectively. Pimecrolimus was dissolved completely in 99.9% DMSO-*d*6 (Eurisotop) as a stock solution of 10 mM.

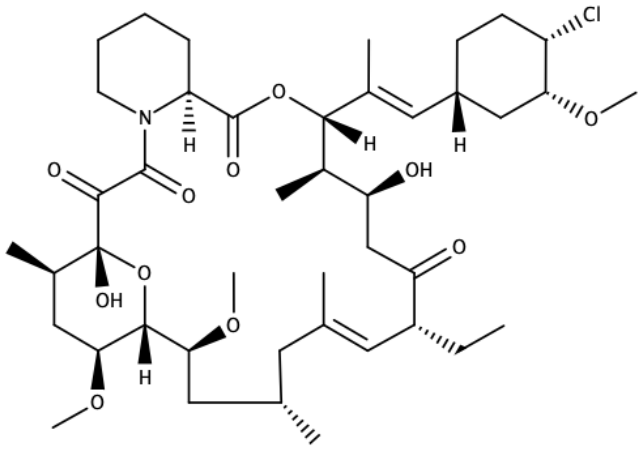

Figure S1. Structural formula of pimecrolimus

1.2 NMR experiments

All NMR measurements were performed on a Bruker AVANCE II 700 (16.4 T) at 25 ˚C; ^{15}N R_2 relaxation dispersion experiments were additionally performed on a Bruker AVANCE III 950 (22.3 T). Both spectrometers were equipped with a 5-mm TCI cryogenic probe and *z*-axis gradient (Bruker). ^{1}H 1D NMR spectra were processed and analyzed by Topspin 4.0.7 software (Bruker); the remaining NMR spectra were processed by NMRPipe[2] and analyzed by using CcpNMR analysis 2.5[3].

2 Analysis of the interaction between FKBP12 and pimecrolimus

2.1 Backbone resonance assignments of pimecrolimus-bound FKBP12

The resonance assignments of free FKBP12 were based on previous reports[4,5]. For pimecrolimus-bound FKBP12, ^{1}H-^{15}N HSQC, HNCO, HN(CA)CO, HN(CO)CA, HNCA, CBCA(CO)NH, HNCACB, and CC(CO)NH spectra[6] were acquired. ^{1}H chemical shifts were referenced to the methyl proton signal of sodium 2,2-dimethyl-2-silapentane-5-sulfonate (DSS; Tokyo Chemical Industry), and ^{13}C and ^{15}N chemical shifts were referenced indirectly[7]. Resonance assignment was performed by using MagRO NMRView[8,9] and FLYA[10].

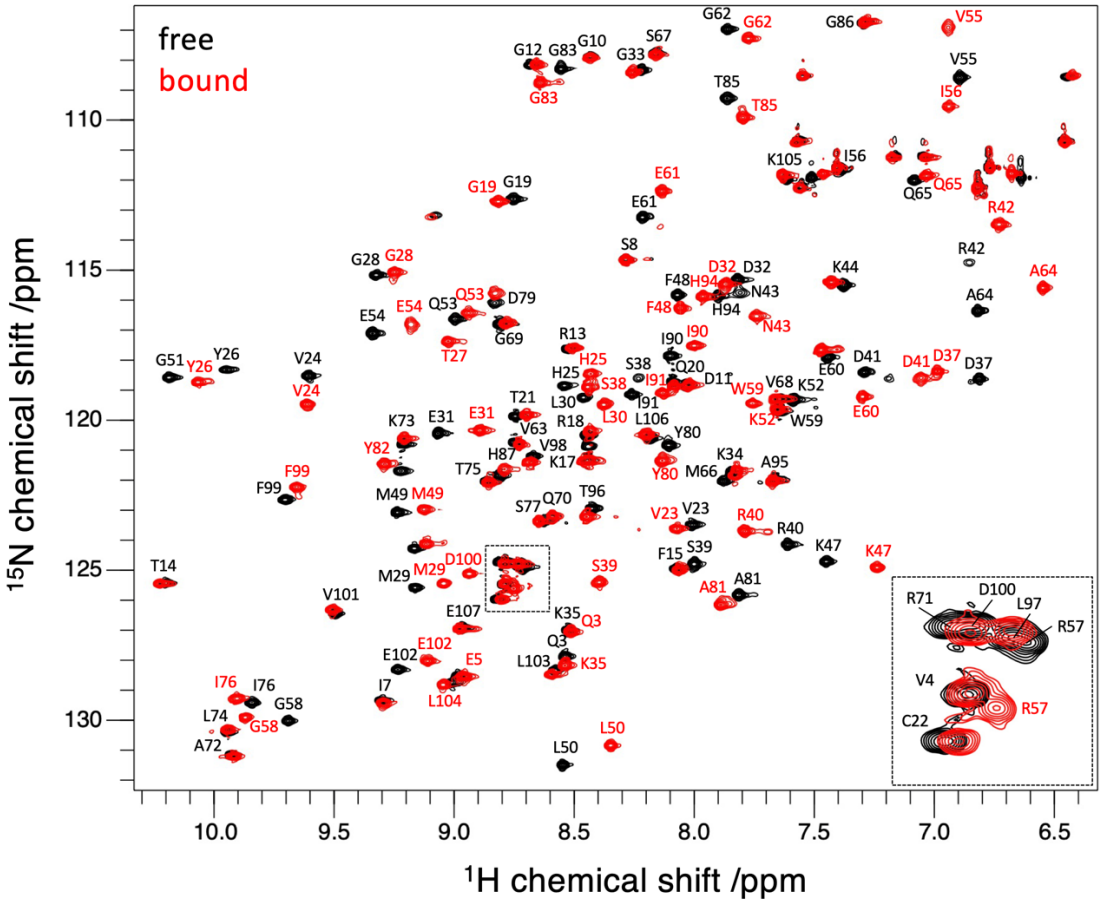

Figure S2. ^{1}H-^{15}N HSQC spectra of FKBP12 in the free state (black) and in the pimecrolimus-bound state (red). Peaks are labeled by the amino acid one-letter code and residue number; in the spectrum of pimecrolimus-bound FKBP12, only peaks with a relatively large chemical shift change upon binding to pimecrolimus are labeled. Eight cross-peaks of free FKBP12 and seven of bound FKBP12 were not assigned due to peak overlap or significant line broadening. For clarity, the crowded region in the spectra is enlarged in the inset.

2.2 Chemical shift differences between free and pimecrolimus-bound FKBP12

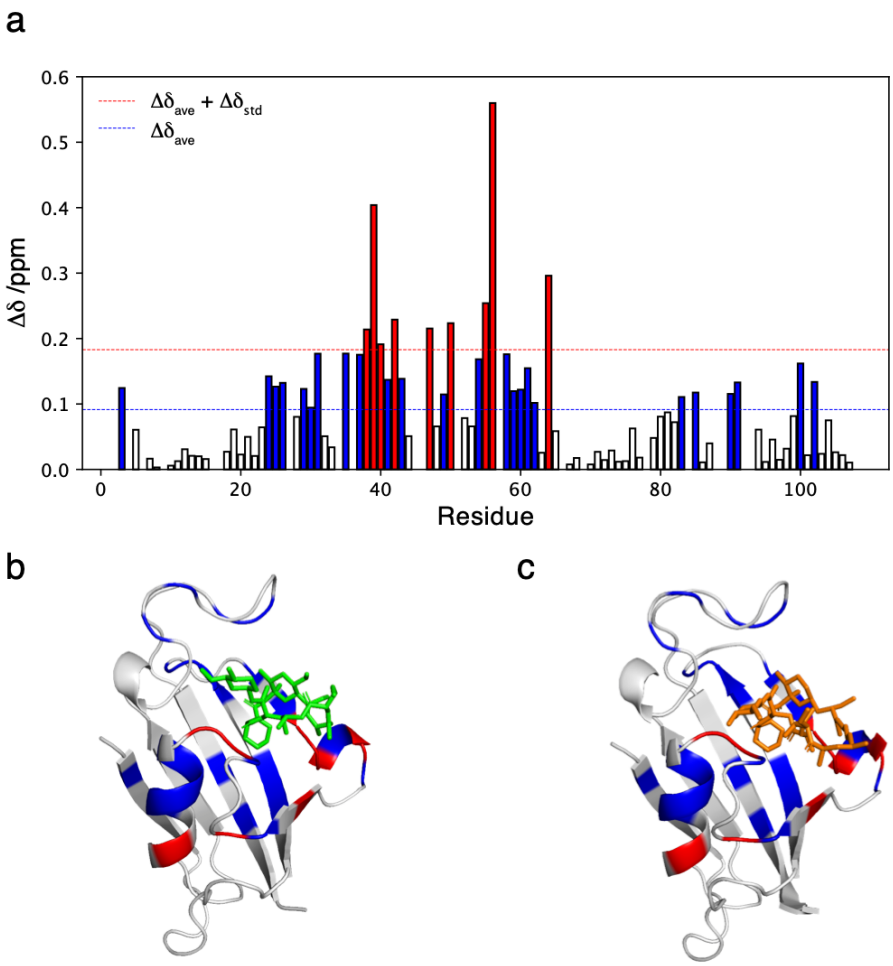

Figure S3. Chemical shift differences between free and pimecrolimus-bound FKBP12 and structural location of FKBP12 residues showing large chemical shift differences. (a) Chemical shift differences (Δδ) between free and pimecrolimus-bound FKBP12. Δδ was calculated as: $\Delta\delta = \sqrt{\Delta\delta_H^2 + (0.15\Delta\delta_N)^2}$, where $\Delta\delta_H$ and $\Delta\delta_N$ are the differences in chemical shift of proton and nitrogen nuclei, respectively. (b) and (c) Δδ mapped onto the crystal structures of the FKBP12–FK506 complex (b, PDB entry 1FKJ) and the FKBP12–Rapamycin complex (c, PDB entry 1FKL). Residues with Δδ larger than the average chemical shift difference ($\Delta\delta_{ave}$) or the average chemical shift difference plus 1 standard deviation ($\Delta\delta_{ave} + \Delta\delta_{std}$) are highlighted in blue or red, respectively. FK506 and rapamycin are shown as, respectively, green and orange sticks. Residues showing relatively large chemical shift changes were found to be located in the vicinity of the binding site of FK506 and rapamycin, suggesting that pimecrolimus associates with FKBP12 via a binding mechanism similar to that used by these two drugs.

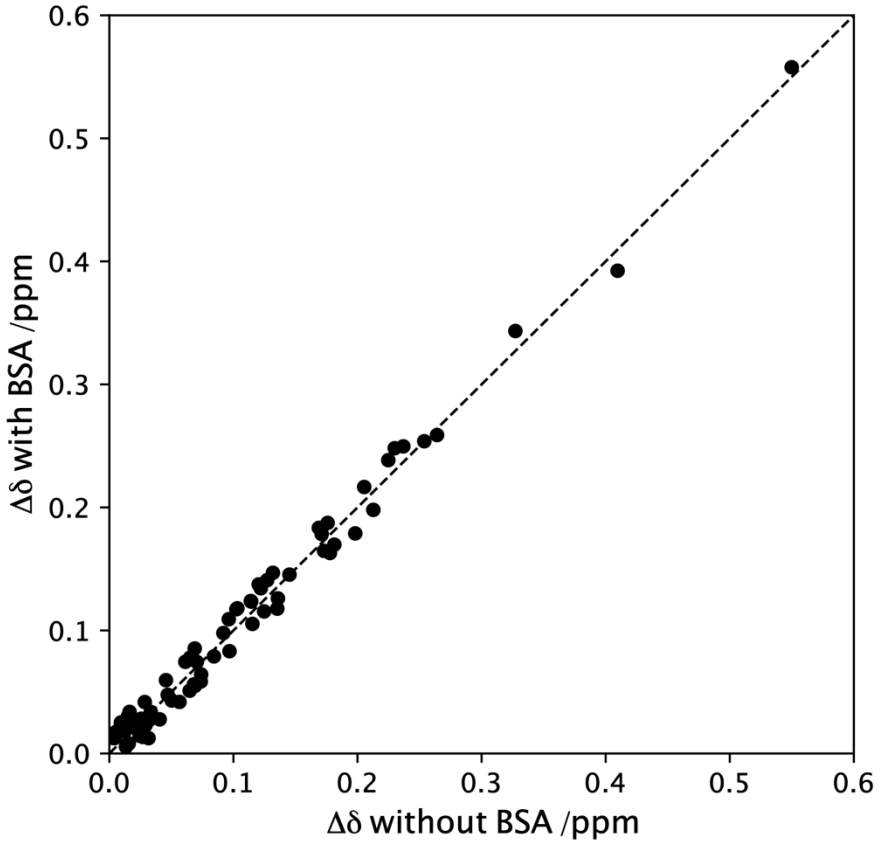

Figure S4. Correlation plot of chemical shift differences between free and pimecrolimus-bound FKBP12 in the presence versus the absence of BSA. The dashed line with a slope of 1 is shown as a guideline.

3 qNMR-aided NMR titration experiment

3.1 Sample preparation

A series of samples for qNMR-aided NMR titration experiments in the dilute and crowded conditions (hereafter referred to as dilute and crowded samples, respectively) were prepared as follows. First, we prepared six mixtures of FKBP12 (320 μM) and pimecrolimus (0, 0.2, 1, 2, 3, and 6 molar equivalents) containing 20% DMSO-*d*6 in Tris buffer (25 mM Tris-HCl, 150 mM NaCl, 0.5 mM tris(2-carboxyethyl)phosphine (TCEP), pH 8.0, 25 ˚C; sample volume: 175 μL). Second, precipitated pimecrolimus was separated from the solution by centrifugation and the precipitated pimecrolimus was dissolved in 99.9% DMSO-*d*6 containing 500 μM DSS-*d*6 (Wako) as an internal reference (hereinafter referred to as the qNMR sample; sample volume: 350 μL). For all samples, centrifugal separation of precipitated pimecrolimus was conducted in the same way (i.e., the same incubation time from mixture preparation to centrifugation) to avoid any unwanted experimental differences caused by differences in equilibrium states between precipitation and dissolution. Finally, the supernatant (175 μL) was used for the dilute and crowded samples, which were prepared by adding an equal volume (175 μL) of either Tris buffer or Tris buffer containing 400 g/L of BSA, respectively. Note that all sample volumes for the NMR titration experiments were set to 350 μL to avoid any unnecessary experimental differences in the NMR measurements.

3.2 Acquisition and processing

The relaxation delay was set to 60 seconds to ensure appropriate T_1 relaxation of all proton resonances. Other parameters were set as follows: number of scans, 32; acquisition time, 4.0 seconds; and spectral width, 14 ppm. In the case that the signal-to-noise (S/N) ratio was insufficient to quantify the concentration of pimecrolimus (i.e., small amount of precipitated pimecrolimus), the number of scans was increased to 256. All spectra were processed with Topspin 4.0.7 software (Bruker) using a line broadening window function (LB = 1.0 Hz) and zero-filling (SI = 262144 points). The phase and baseline of the spectra were automatically or manually corrected. The chemical shifts of all spectra were calibrated based on the methyl proton signal of DSS-*d*6.

3.3 Integration

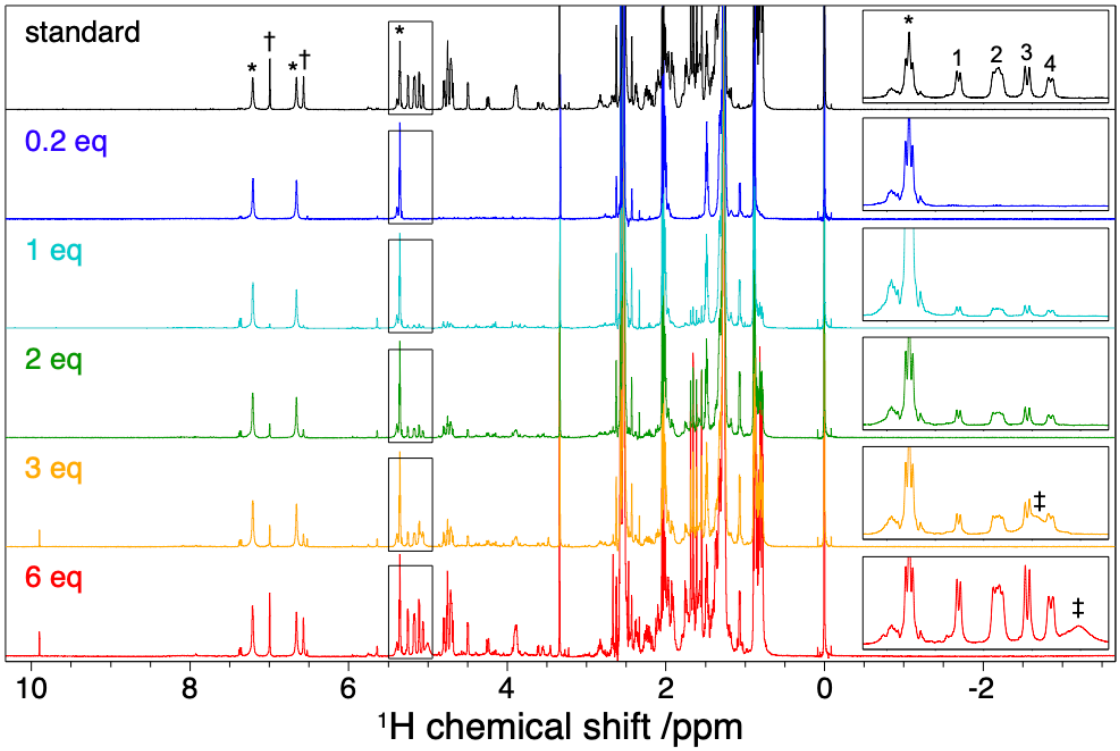

Figure S5. 1D ^{1}H NMR spectra of pimecrolimus (resolubilized in DMSO-*d*6) precipitates obtained from centrifugation of solutions containing 160 μM FKBP12 and 0.2, 1, 2, 3, and 6 molar equivalents of pimecrolimus (blue, cyan, green, orange, and red, respectively) to FKBP12 and the pimecrolimus standard sample (500 μM; black) dissolved in DMSO-*d*6. Insets display enlarged views of the signals of pimecrolimus with a high S/N ratio. Because many peaks of pimecrolimus were not assigned owing to severe overlap, we identified peaks by numbers, in the insets. Those labeled with asterisks, daggers, and double daggers were removed from the analysis because they corresponded to impurity peaks in DMSO-*d*6, exchangeable peaks of pimecrolimus (hydroxyl protons), and buffer (Tris)-derived peaks, respectively. Hydroxyl proton signals were identified by the addition of D_2O. The broad signal of Tris (double daggers) was observed in some spectra (orange and red) and overlapped with signals of pimecrolimus (peaks 3 and 4). Moreover, signal 1 slightly overlapped with that of the DMSO-*d*6 impurity (asterisks), which would lead to an inaccurate estimation of pimecrolimus concentration, especially in spectra with a relatively low S/N ratio (1 and 2 equimolar samples). For these reasons, we decided to use signal 2 in the qNMR calculation. For quantitative assessment, the integrated signal intensity of pimecrolimus was normalized to the DSS-*d*6 signal intensity.

3.4 Residual FKBP12 contained in precipitated pimecrolimus

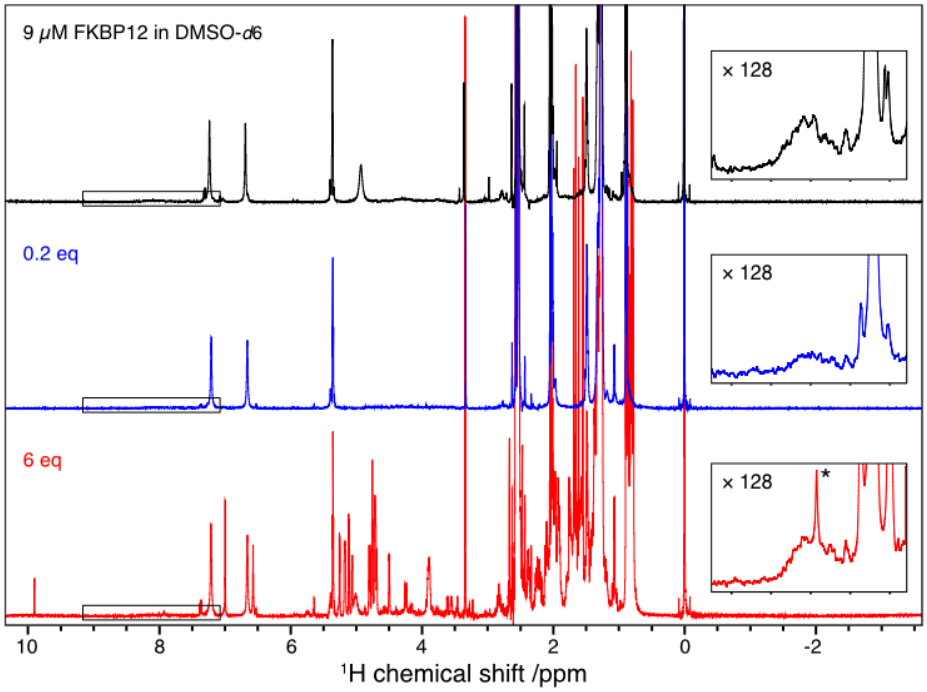

Figure S6. 1D ^{1}H NMR spectra of pimecrolimus (resolubilized in DMSO-*d*6) precipitates obtained from centrifugation of solutions containing 160 μM FKBP12 and 0.2 (blue) and 6 (red) molar equivalents of pimecrolimus to FKBP12 (160 μM) and 9 μM FKBP12 dissolved in DMSO-*d*6 (black). We found in all spectra limited ^{1}H NMR signals around 7–9 ppm that are derived from $^{1}H^{N}$ backbone resonances of FKBP12, indicating that the precipitates contain a limited amount of FKBP12; insets display enlarged views of these signals (an asterisk indicates the peak of pimecrolimus). The residual FKBP12 contained in the precipitates is likely to be due to incomplete centrifugal separation of solids and liquids because buffer (Tris, a very soluble molecule)-derived NMR signals were also observed in ^{1}H NMR spectra of the pimecrolimus precipitates (Fig. S5). By ^{1}H-qNMR using 9 μM FKBP12 in DMSO-*d*6 as a standard sample, we quantified the amount of the residual FKBP12 contained in the pimecrolimus precipitates, obtaining the result that the precipitates in all samples contained approximately 2 % of total amount of FKBP12. Namely, without consideration of the residual FKBP12, the total concentration of FKBP12 ($[F_{total}]$) is 2 % overestimated; however, this leads to negligible underestimation of K_d based on accuracy of their values (error values). Therefore, the residual FKBP12 in pimecrolimus precipitates was not considered in the downstream analyses.

3.5 Linearity

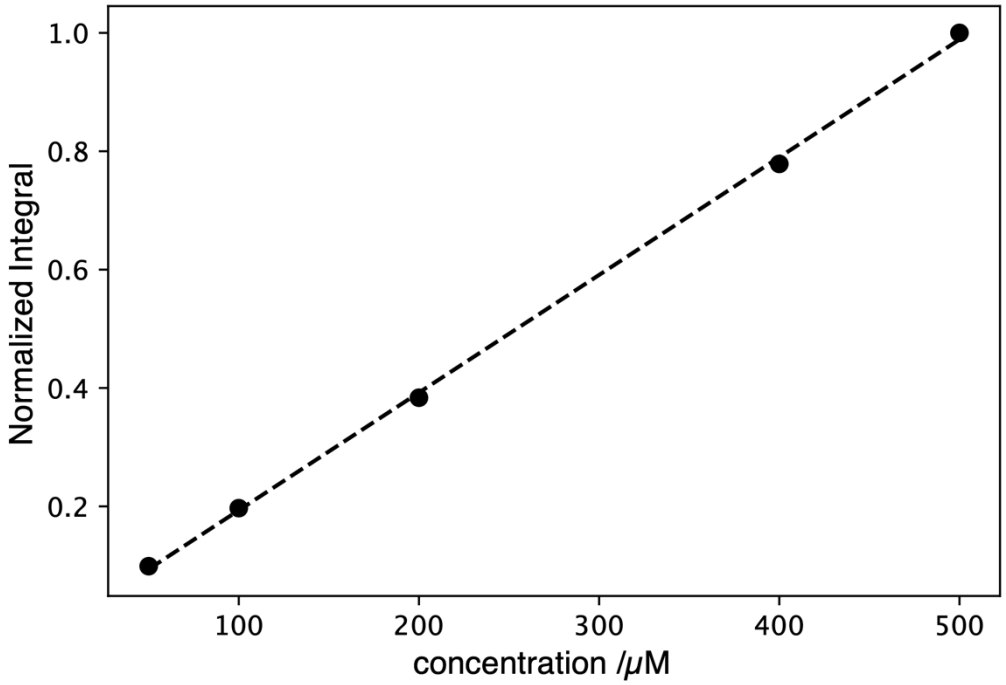

Figure S7. Linearity of the concentration determined by qNMR. Shown is a linear plot of concentration versus integral value in the pimecrolimus concentration range of 50, 100, 200, 400, and 500 μM. Good linearity was achieved: the regression equation was [Normalized Integral] = 0.002 × [Concentration] – 0.005, with a coefficient of determination of $R^2 = 0.99$.

3.6 qNMR-aided NMR titration in the crowded condition

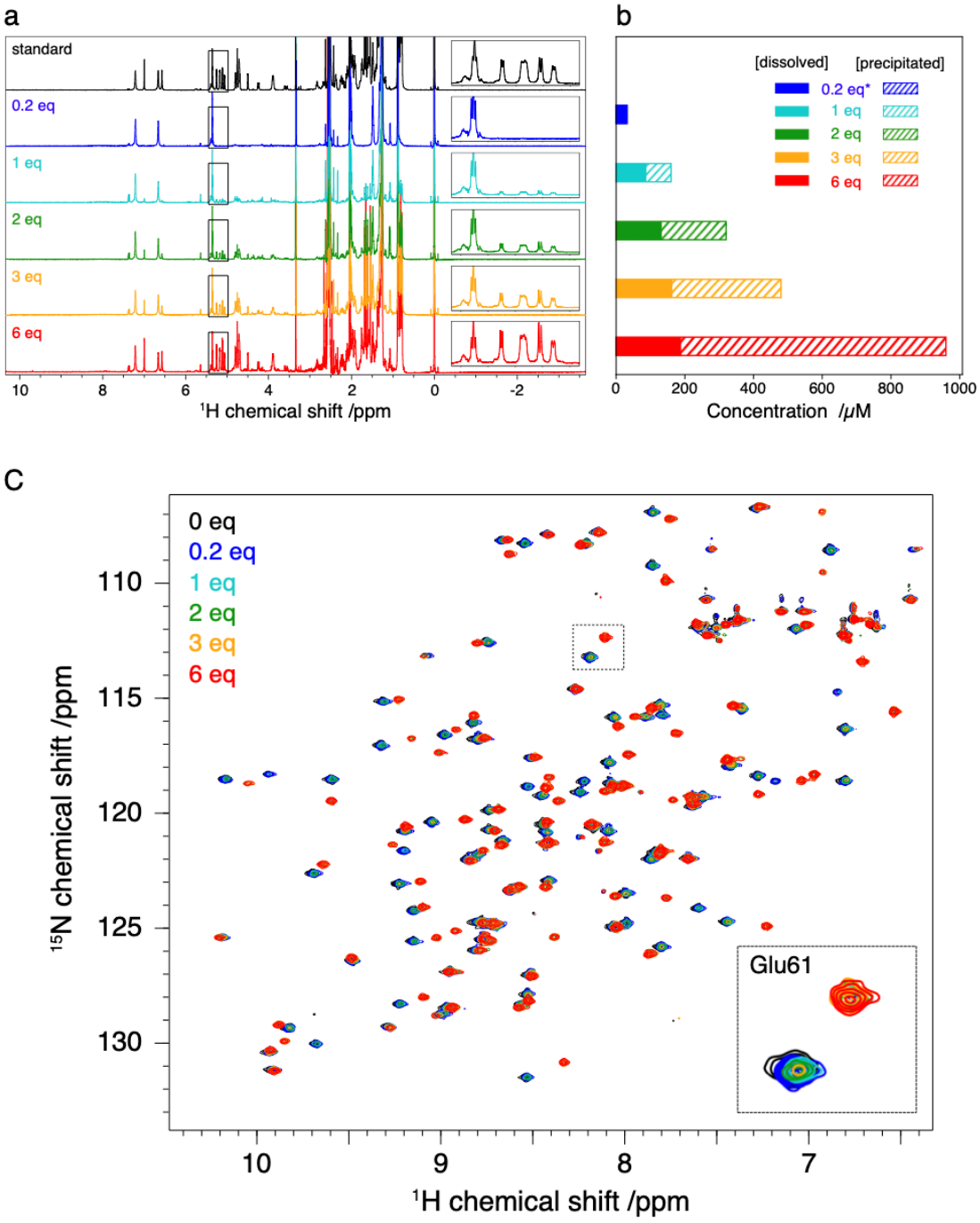

Figure S8. (a) 1D ^{1}H NMR spectra of precipitated pimecrolimus in solutions containing FKBP12 and 0.2, 1, 2, 3, and 6 molar equivalents of pimecrolimus (blue, cyan, green, orange, and red, respectively) of the crowded samples and pimecrolimus standard sample (500 μM; black) dissolved in DMSO-*d*6. Insets display enlarged views of the signals of pimecrolimus with a good S/N ratio. (b) Stacked bar graph of the concentration of dissolved pimecrolimus (solid bars) and that of precipitated pimecrolimus (hatched bars)

for each sample. *The pimecrolimus signal was not observed in the 1D ^{1}H NMR spectrum of the sample prepared as “precipitated” pimecrolimus; therefore, pimecrolimus was regarded as completely dissolved in this sample. (c) ^{1}H-^{15}N HSQC spectra of [*U*-^{15}N]-FKBP12 with different concentrations of pimecrolimus (0, 0.2, 1, 2, 3, and 6 molar equivalents to FKBP12: black, blue, cyan, green, orange, and red, respectively) in the crowded condition. Inset shows an enlarged view of a representative peak that changed in intensity due to the addition of pimecrolimus (residue Glu61).

3.7 Calculated concentrations

Table S1 Concentrations of dissolved pimecrolimus and pimecrolimus-bound FKBP12 in the titration samples

$[P_{total}]$ /μM	$[P_{dissolved}]$ /μM[a]		average $[F_{bound}]$ /μM[c]	
	Dilute	Crowded	Dilute	Crowded
32	32[b]	32[b]	24 ± 5	25 ± 5
160	112 ± 2	88 ± 1	101 ± 8	75 ± 8
320	136 ± 2	133 ± 1	133 ± 5	100 ± 6
480	229 ± 2	164 ± 2	148 ± 3	131 ± 6
960	225 ± 4	189 ± 7	160[d]	160[d]

[a]Data are the average and standard deviation of 3 measurements.

[b]The pimecrolimus signal was not observed in the 1D ^{1}H NMR spectrum of the sample prepared as "precipitated" pimecrolimus; therefore, pimecrolimus was regarded as completely dissolved in this sample (i.e., $[pimecrolimus_{dissolved}] = 32$ μM)

[c]Average $[F_{bound}]$ was calculated using $[F_{bound}]$ values of all the residues showing CSP larger than average CSP except for the residues whose peaks are overlapped with other peaks.

[d]Because the peaks of free FKBP12 were not observed at $[P_{total}]$ of 960 μM for all residues used to calculate the average $[F_{bound}]$, $[F_{bound}]$ was estimated to be the total concentration of FKBP12, namely 160 μM.

3.8 Titration curve fitting

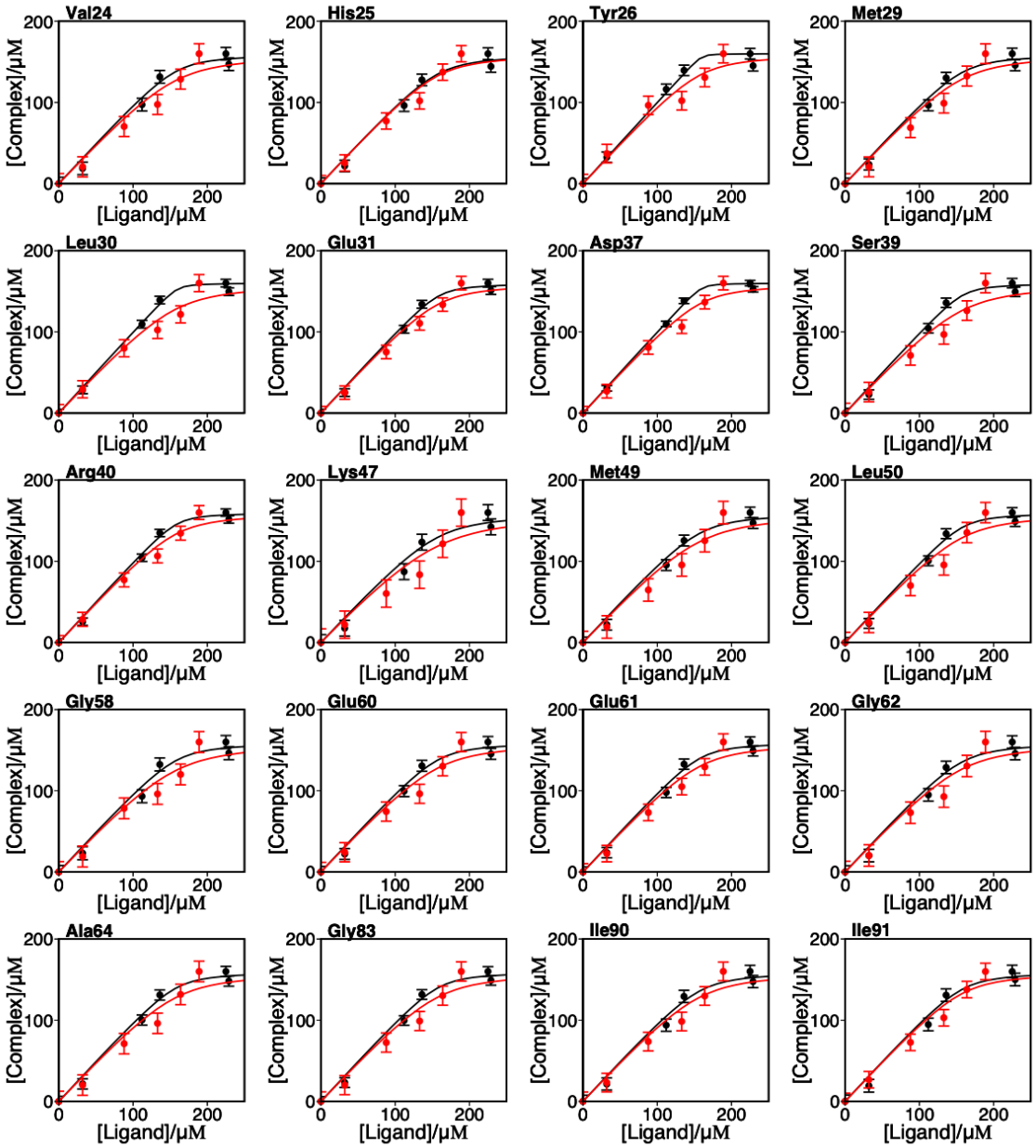

Figure S9. Local curve fitting for the FKBP12 residues that showed relatively large chemical shift changes on binding to pimecrolimus in dilute (black) and crowded (red) conditions, yielding residue-resolved K_d (Fig. S10). Error bars denote the fitting error[11].

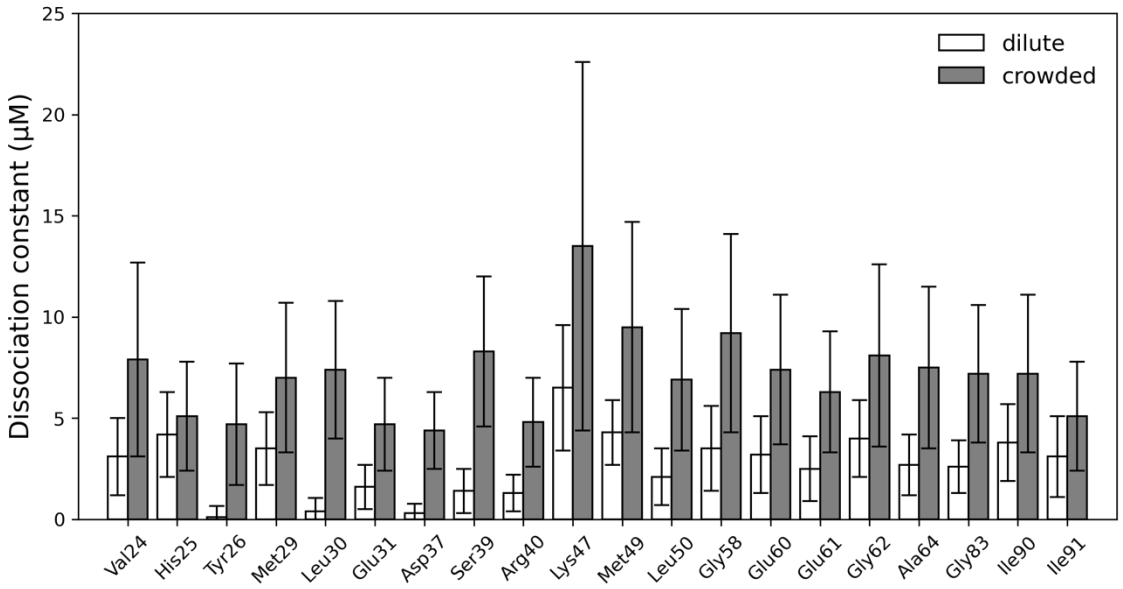

Figure S10. Bar graph of residue-resolved K_d both in dilute (white) and crowded (gray) conditions. Standard deviations of the fitting parameters were estimated by the Monte Carlo method (100 iterations).

4 Analysis of the interaction between pimecrolimus and BSA

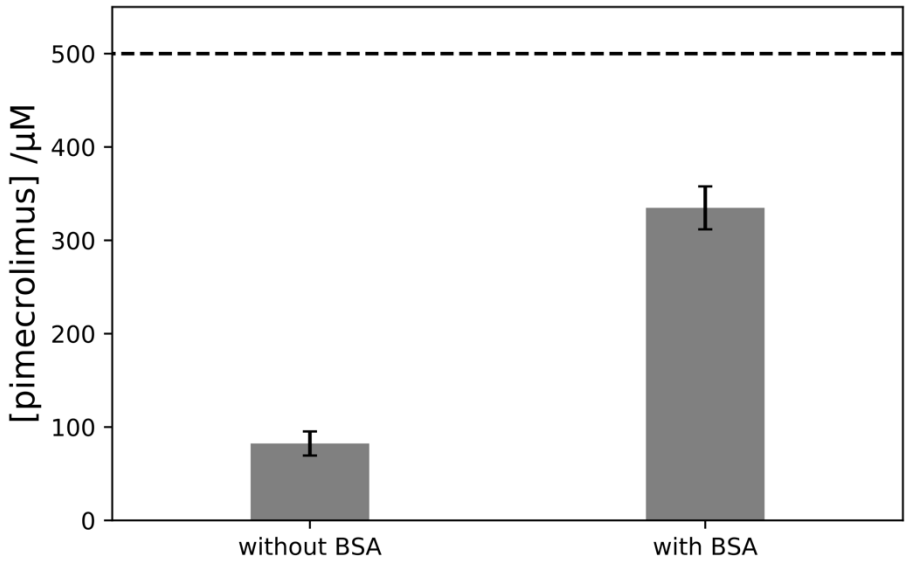

Figure S11. Solubility of pimecrolimus enhanced by nonspecific interactions with BSA. The bar graph shows the concentrations of dissolved pimecrolimus in the absence and presence of BSA. Pimecrolimus was dissolved in Tris buffer (pH 8.0 at 25 ˚C) at a concentration of 500 µM in the presence and absence of 200 g/L BSA, and then dissolved pimecrolimus was quantified by qNMR. The dashed line denotes the total concentration of pimecrolimus. Error bars represent the uncertainties as estimated from duplicate measurements.

5 R_2 relaxation dispersion experiment

5.1 Experimental details

For the ^{15}N R_2 relaxation dispersion experiment, we prepared samples of 500 μM [*U*-^{15}N]-FKBP12 with and without 1 molar equivalent of pimecrolimus in Tris buffer or Tris buffer containing 200 g/L BSA. R_2 relaxation dispersion experiments[12,13] were performed at magnetic field strengths of 16.4 T and 22.3 T in the dilute and crowded conditions. The constant CPMG time T_{CPMG} was set to 50 milliseconds and the CPMG pulse frequencies $1/\tau_{CP}$ ranged from 40 to 2000 s^{-1}. Effective transverse relaxation rates (R_2^{eff}) were calculated as: $R_2^{\mathrm{eff}}\left(1/\tau_{\mathrm{cp}}\right) = -\frac{1}{T}\ln\frac{I}{I_0}$, where I and I_0 are peak intensities in, respectively, the presence and absence of the CPMG pulse train. The intrinsic transverse relaxation rate (R_2^0) for all residues increased almost uniformly throughout the whole protein sequence in the BSA-crowded condition (Figure S13), but R_{ex} remained almost unchanged for all residues (Figure S14). This means that concentrated BSA mainly contributed to an increase in the viscosity of the solution. In other words, the interaction between BSA and FKBP12 can be neglected in the analysis of the R_2 relaxation dispersions. Therefore, the R_2 relaxation dispersions were fitted to a model of two-state exchange between the free and bound states using the program GLOVE[14]. Because the chemical shift differences between free and pimecrolimus-bound FKBP12 in the BSA-crowded condition were almost the same as those in the absence of BSA (Figure S4), the chemical shift difference ($\Delta\omega$) of each residue in the dilute and crowded conditions was shared in the fitting of the R_2 dispersion curves. Standard deviations of the fitting parameters were estimated by the Monte Carlo method (100 iterations).

5.2 The effects of macromolecular crowding

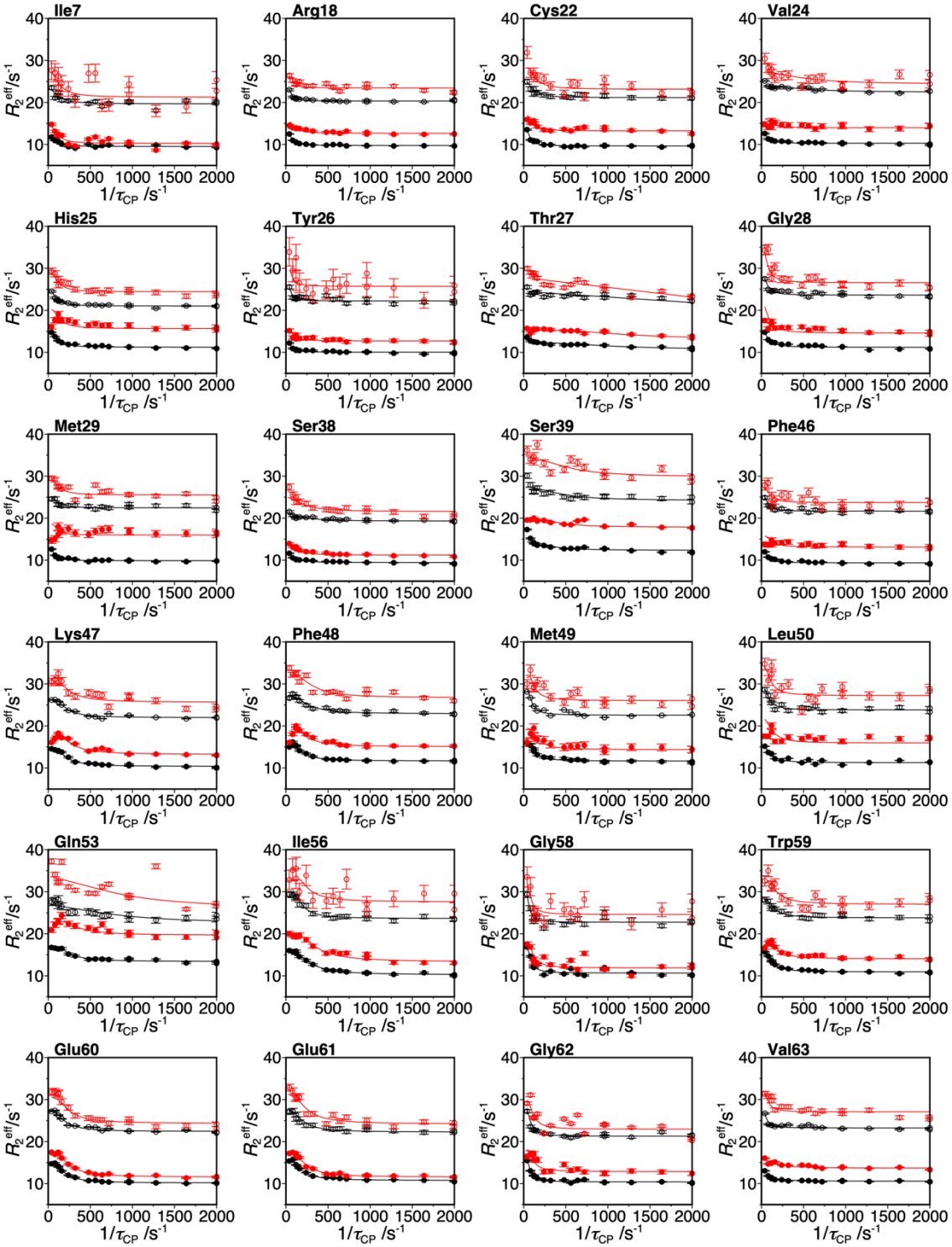

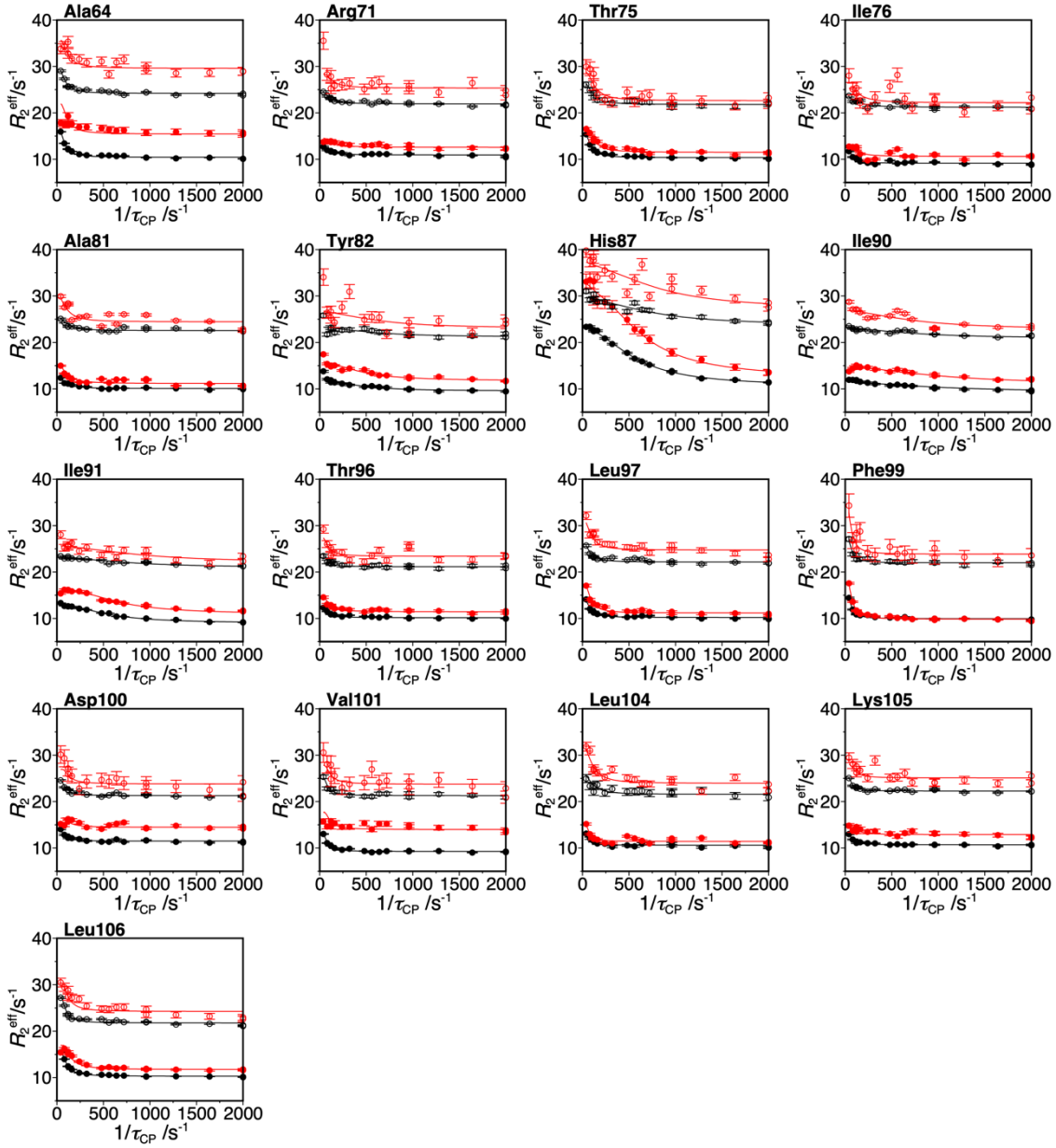

Figure S12. R_2 relaxation dispersion profiles (shown are residues with $R_{ex} > 2$ s^{-1} at the magnetic field strength of 16.4 T) of pimecrolimus-bound FKBP12 at magnetic field strengths of 16.4 T (black) and 22.3 T (red) in the dilute (filled circles) and crowded (open circles) conditions. Error bars represent the uncertainties as estimated from duplicate measurements.

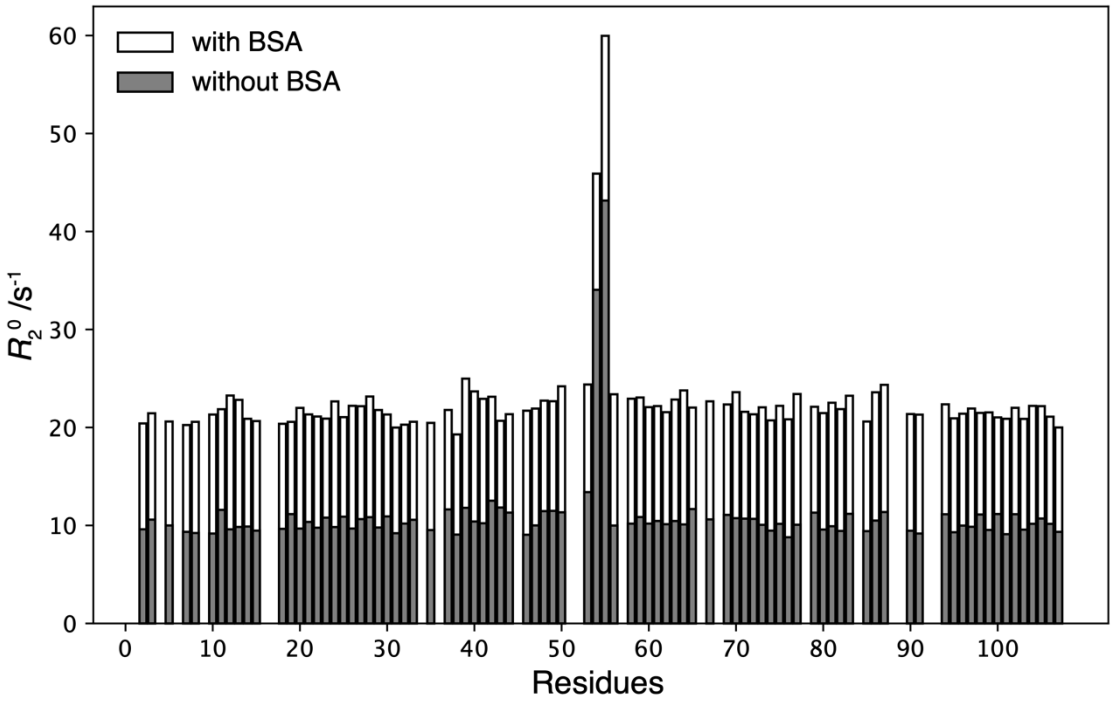

Figure S13. Comparison of the intrinsic transverse relaxation rates (R_2^0) of FKBP12 in the presence (white bars) and absence (gray bars) of BSA.

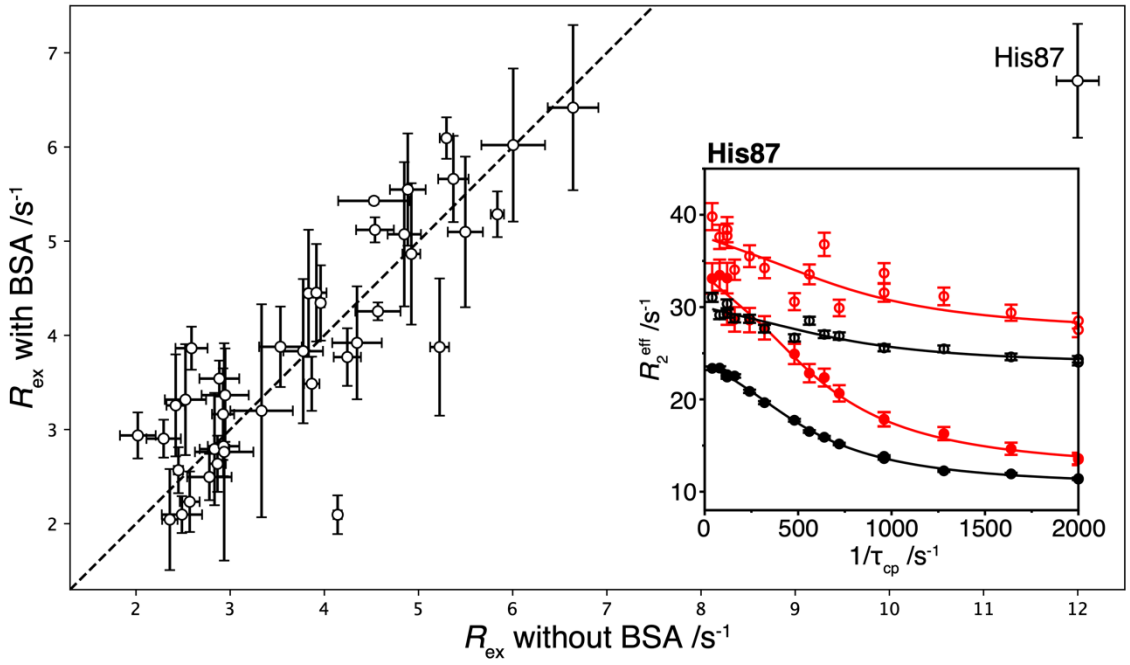

Figure S14. Correlation plot of the derived R_{ex} (> 2 s^{-1}) values at a magnetic field strength of 16.4 T in the dilute versus the crowded condition. The dashed line with a slope of 1 is drawn as a guideline. Inset shows the R_2 relaxation dispersion profiles of His87 at magnetic field strengths of 16.4 T (black) and 22.3 T (red) in the dilute (filled circles) and crowded (open circles) conditions. The R_{ex} values obtained in the presence of BSA are well correlated with those derived in the absence of BSA except for His87, indicating that local structural fluctuations of His87 in the bound state are affected due to the presence of BSA (i.e., in the crowded condition).

5.3 Global analysis

R_2 relaxation dispersion data for 4 residues reporting on the main binding site on FKBP12 (Glu61, Ala81, Thr96, and Phe99) were used for global fitting, under the assumption that these residues share the same association and dissociation rates. The chemical shift differences of these (binding site-adjacent) residues (|Δω|; as determined from fitting the R_2 relaxation dispersion data to the two-state exchange model) were well correlated with those obtained from the HSQC spectra (|Δδ|) (Figure S15), confirming that the observed R_2 relaxation dispersion was indeed caused by chemical exchange between the free and bound states. We note that many of the remaining residues showed no linear correlation between Δω and Δδ, suggesting the existence of another process such as conformational exchange in the bound state.

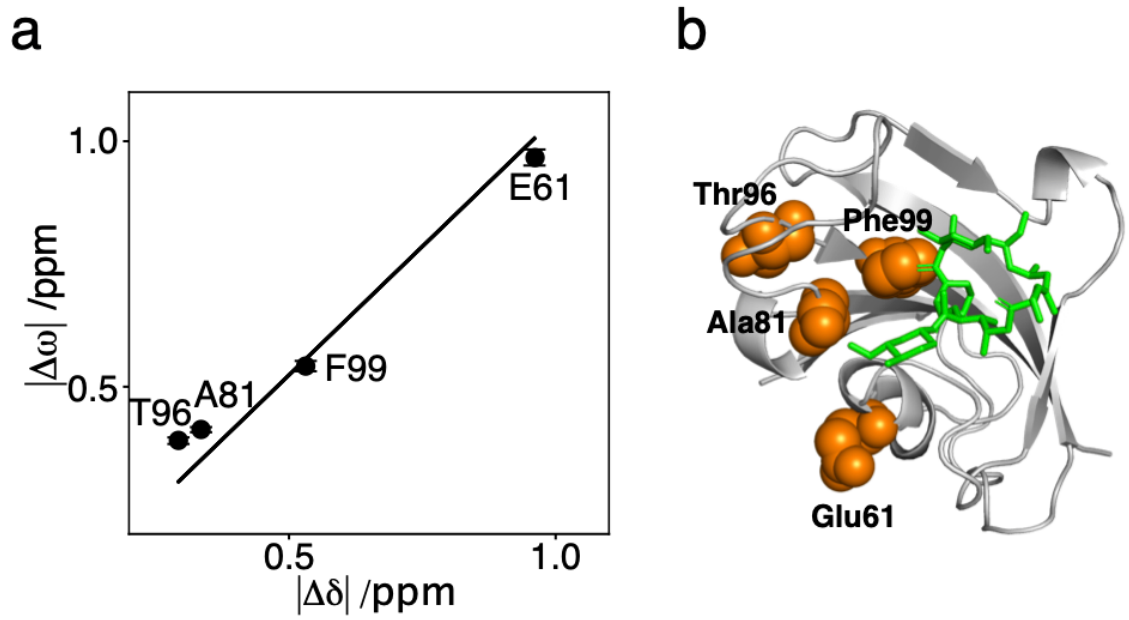

Figure S15. Global analysis of R_2 relaxation dispersion data. (a) Correlation plot of ^{15}N chemical shift differences determined from R_2 relaxation dispersion data (|Δω|) versus those from HSQC spectra (|Δδ|). A linear correlation was observed with a slope of 1.05 and R^2 of 0.99. (b) Crystal structure of the FKBP12–FK506 complex (PDB entry 1FKJ; FK506 is shown as a green stick), in which the 4 residues (Glu61, Ala81, Thr96, and Phe99) used for global fitting are shown as orange spheres.

1 D. Morimoto, E. Walinda, H. Fukada, K. Sugase and M. Shirakawa, *Sci. Rep.*, 2016, **6**, 1–9.

2 F. Delaglio, S. Grzesiek, G. W. Vuister, G. Zhu, J. Pfeifer and A. Bax, *J. Biomol. NMR*, 1995, **6**, 277–293.

3 W. F. Vranken, W. Boucher, T. J. Stevens, R. H. Fogh, A. Pajon, M. Llinas, E. L. Ulrich, J. L. Markley, J. Ionides and E. D. Laue, *Proteins Struct. Funct. Bioinforma.*, 2005, **59**, 687–696.

4 S. M. Mustafi, H. Chen, H. Li, D. M. Lemaster and G. Hernández, *Biochem. J.*, 2013, **453**, 371–380.

5 S. M. C. Gobeil, B. G. Bobay, L. D. Spicer and R. A. Venters, *Biomol. NMR Assign.*, 2019, **13**, 207–212.

6 M. Sattler, J. Schleucher and C. Griesinger, *Prog. Nucl. Magn. Reson. Spectrosc.*, 1999, **34**, 93–158.

7 J. L. Markley, A. Bax, Y. Arata, C. W. Hilbers, R. Kaptein, B. D. Sykes, P. E. Wright and K. Wüthrich, *Eur. J. Biochem.*, 1998, **256**, 1–15.

8 B. A. Johnson and R. A. Blevins, *J. Biomol. NMR*, 1994, **4**, 603–614.

9 N. Kobayashi, J. Iwahara, S. Koshiba, T. Tomizawa, N. Tochio, P. Güntert, T. Kigawa and S. Yokoyama, *J. Biomol. NMR*, 2007, **39**, 31–52.

10 E. Schmidt and P. Güntert, *J. Am. Chem. Soc.*, 2012, **134**, 12817–12829.

11 L. K. Nicholson, D. M. Baldisseri, D. A. Torchia, L. E. Kay, J. Arango and P. E. Young, *Biochemistry*, 1992, **31**, 5253–5263.

12 J. P. Loria, M. Rance and A. G. Palmer, *J. Am. Chem. Soc.*, 1999, **121**, 2331–2332.

13 S. D. Chatterjee, M. Ubbink and H. van Ingen, *J. Biomol. NMR*, 2018, **71**, 69–77.

14 K. Sugase, T. Konuma, J. C. Lansing and P. E. Wright, *J. Biomol. NMR*, 2013, **56**, 275–283.